AIAA 80-0328R

Rational Design of an Airfoil for a High-Performance Jet Trainer

S.A. Powers* and D.F. Sattler†
The Vought Corporation, Dallas, Texas

This paper discusses the design of an airfoil for a high-performance jet trainer. The airfoil design requirements are discussed and related to the aircraft performance requirements. The rationale for the pressure distribution model is outlined. The use of the airfoil design program in converting the pressure distribution model into an airfoil is discussed and the results presented. The indications are that the resulting airfoil will have the desired characteristics.

Nomenclature

ac = aerodynamic center, % chord
c = chord length, ft
c_l = section or two-dimensional lift coefficient
C_L = vehicle or three-dimensional lift coefficient
C_p = ordinary pressure coefficient
$\bar{C}_p$ = pressure coefficient referred to rooftop condition, $(P-P_r)/(P_{stag}-P_r)$
F = intermediate function defined for Eq. (3)
M = Mach number
n = exponent of "super-ellipse" equation, Eq. (1)
n_s = $\log(R_s)$
P = pressure, lb/ft^2
R = Reynolds number, $\rho uc/\mu$
x = distance along the chord, measured from the leading edge, ft
x^* = distance along the chord, measured from the virtual origin of the turbulent boundary layer, ft
δ^* = boundary-layer displacement thickness, ft

Subscripts

l = lower surface condition
r = rooftop conditions
s = separation conditions
stag = stagnation conditions
te = trailing-edge conditions
∞ = freestream conditions
u = upper surface condition

Introduction

VOUGHT Corporation was one of four contractors chosen by NADC to study advanced undergraduate pilot training systems. This work was carried out between March and October 1978. The Vought study concentrated on reducing the system life cycle cost and the fuel consumption of the aircraft to the lowest possible levels. In order to achieve low system life cycle costs, the aircraft itself must be small in order to reduce production costs, and the aircraft fuel usage must be low to reduce the operating costs. In order to minimize the cost and fuel consumption of the Vought aircraft, a specialized airfoil was needed. The preliminary design of the airfoil was undertaken to provide technical data needed for the aircraft design. This paper discusses this airfoil design effort.

At the outset of this study, it was recognized that good transonic airfoil analysis and design computer programs were available and their use was acceptable to knowledgeable technical people within Vought and the Navy. The Bauer, Garabedian, and Korn[1] and Carlson[2] analysis programs and their design option versions[3,4] are well known and widely accepted. The programs can be used effectively to determine special-purpose airfoils if the proper design criteria are used. The approach used in this study was to determine a rational set of design requirements for the airfoil, develop a pressure distribution model aimed at satisfying these design requirements, and then use one of the design programs to develop the airfoil geometry. A limited exploration of the off-design characteristics of the final profile was also carried out.

The following discussion is intended to illuminate the process used in designing the airfoil. The final results themselves are still somewhat tentative in nature and will change with further development. However, the process does succeed in providing an airfoil with the required performance for this specialized need.

Requirements

Aircraft Design Requirements

The aircraft for which the airfoil was to be designed was required to be as small and as light as possible in order to reduce the life cycle costs to a minimum. Most of the aircraft design requirements were stated as threshold/goal pairs. After some initial exploratory studies, Vought chose to design to the goals in all but one case (the goal value for maximum Mach number was not used). The aircraft performance requirements influencing the airfoil design were:

1) The aircraft was to be subsonic, but with good transonic characteristics (M_{max} greater than or equal to 0.8).

2) The aircraft approach speed was to be 105 knots.

3) The aircraft was to be capable of sustained 4 g turns at 15,000 ft.

4) The aircraft was to be spinnable and recoverable.

5) The aircraft was to have a 150 n.mi. radius on a hi-lo-lo-hi training mission.

An aircraft with a maximum level flight Mach number of 0.8 or greater will be able to achieve transonic and possibly supersonic flight in dives. It was therefore deemed important that the occurrence of shock waves be delayed as long as possible and that Mach tuck characteristics be minimized. Note that a high value of drag divergence Mach number was not considered necessary. From a configuration point of view, the characteristics of the tail airfoil section are also of interest in insuring good transonic characteristics. However, that problem is outside the purview of this paper.

In order to generate a low approach speed, the airfoil geometry must be compatible with a powerful flap system. In order for this flap system to develop the largest possible lift, the airfoil leading edge must have a large radius of curvature or be flapped, or both. The airfoil geometry must be capable of housing the flap and most of the flap operating mechanism. These requirements imply that the airfoil should be as thick as possible, with a large nose radius.

Received Jan. 9, 1980; presented as Paper 80-0328 at the AIAA 18th Aerospace Sciences Meeting, Pasadena, Calif., Jan. 14-16, 1980; revision received Feb. 17, 1981.

*Project Engineer. Member AIAA.
†Senior Engineer.

In order to sustain 4 g at 15,000 ft, early studies indicated that the aircraft C_L would be slightly over 0.5 at $M_\infty = 0.7$, placing the airfoil performance in the lower transonic region. As will be shown later in this paper, a standard NACA 6-series airfoil develops a midchord shock at this condition. In order to provide the best performance and handling characteristics, the wing should be shock and buffet free at this flight condition.

For an aircraft to have predictable spinning characteristics, among other things, the wing airfoil should have a well-behaved stall. The stall should be of the progressive trailing-edge variety in order that the loss of C_L is not abrupt and/or startling. An airfoil with a large nose radius and a progressive trailing-edge stall should provide these characteristics.

The low-level design mission required that over half of the internal fuel be expended at very low lift coefficients (C_L values on the order of 0.1). This consideration underscores the importance of having both a low zero lift profile drag coefficient and a low variation of profile drag coefficient with lift coefficient.

Early design studies predicted that the optimum wing thickness from the aircraft point of view was about 12%. Lower thickness values increased the amount of structural material needed to handle the loads; larger thickness resulted in weight increases due to the use of minimum gage skins in the wing structure and the growth of the total drag of the aircraft.

Airfoil Design Requirements

The approach to choosing an airfoil for a military trainer is complicated by the wide range of conditions over which the aircraft must operate. A military trainer is used in mock air combat, aerobatics, bombing, gunnery, low-level dashes, etc. Therefore, no one flight condition represents a clear design point. The usual design process selects an airfoil for a cruise condition and checks the performance at off-design conditions. In this study, we chose to design an airfoil for the sustained-turn condition, and then checked the off-design operation at cruise.

The family of airfoils developed by Liebeck[5] were considered for this design. These airfoils have remarkably low values and rates of growth of profile drag, in addition to their high $C_{L_{max}}$ values. However, the stall characteristics were considered to be too abrupt for use on a manned aircraft and the transonic performance was considered inadequate.

Reference 6 discusses rooftop-type airfoils with linear recompression gradients and separation fixed at the trailing edge. These rooftop airfoils allow the upper surface to provide the largest possible contribution to the airfoil lift for a given limit on upper surface Mach number M_r. Also, by limiting M_r to 1.03 or less, shockfree recompression is possible. Producing these airfoils with a linear recompression gradient and separation at the trailing edge for the design point should provide a low profile drag and allow the stall to develop gradually from the trailing edge. This type of pressure distribution appeared to offer the greatest potential for the least technical risk. It was then decided to design a special airfoil using this approach to the shock and separation problems.

After some preliminary investigation the trainer airfoil design requirements were then given as:

1) Shockfree for $c_l = 0.52$ at $M = 0.7$ at 15,000 ft.

2) Separation fixed at the trailing edge for these conditions.

3) Linear recompression region from the rooftop to the trailing edge.

4) Thickness of 12%.

5) Largest possible nose radius.

Pressure Distribution Model

Nose Region

Following the lead of Ref. 6, a rooftop-type pressure distribution was used. Since a large nose radius of curvature is desirable for low-speed considerations, some control over the nose radius was needed. A parametric pressure distribution was evaluated for the nose region which allowed variation in nose radius. From the leading edge to the theoretical ramp break point, the pressure was to be prescribed by a "super-ellipse" equation:

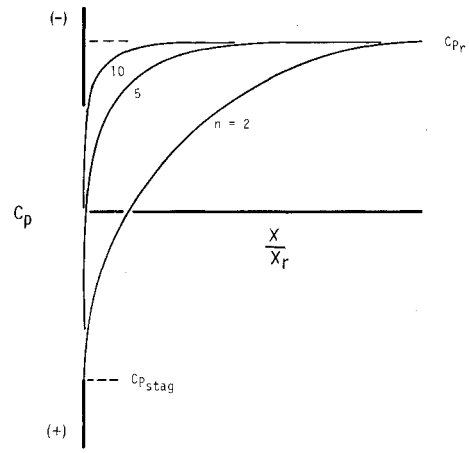

Fig. 1 Nose pressure distributions.

$$\left[\frac{C_p - C_{p_{stag}}}{C_{p_r} - C_{P_{stag}}}\right]^n + \left[1 - \frac{x}{x_r}\right]^n = 1 \tag{1}$$

where the value of the exponent n was a free variable. As shown in Fig. 1, the shape of the curve can be varied from elliptical for $n = 2$ to almost rectangular for n greater than 10. The nose radius was expected to be a function of the exponent n. Small values of n were expected to provide small nose radii, and vice versa.

The upper surface minimum pressure coefficient C_p was set by limiting the maximum ramp Mach number M_r to a value of 1.03. Reference 6 states that this is the maximum Mach number from which isentropic recompression can be achieved. Obviously the value of M_r should be as low as possible to reduce the possibility of shock waves in the recompression region, and as high as possible to enhance the lift generation capability of the airfoil. A balance of these two requirements is needed.

Trailing-Edge Region

Reference 6 suggested that the Stratford criterion[7] be reinterpreted and rearranged to prescribe a linear aft recompression ramp for which separation occurs at the trailing edge at the airfoil design condition. Thus, separation would be unlikely to occur at lower angles of attack and, when it does occur, it will begin at the trailing edge and move forward.

The Stratford criterion for the separation of turbulent boundary layers is:

$$\left(2\bar{C}_{P_s}\right)^{0.25(n_s+2)}\left[x^*\frac{d\bar{C}_{P_s}}{dx^*}\right]^{0.5} = 1.05\left[0.774\left(10^{-6}R_s\right)^{0.1}\right] \tag{2}$$

Here the factor of 1.05 suggested by Wilkinson[8] has been used on the right-hand side, as well as his interpretation of the equation for compressible flows. Note that the pressure coefficient is referenced to the conditions on the airfoil rooftop and that the distance x^* is referenced to the virtual origin of the turbulent boundary layer. As shown in Ref. 6, if the derivative in Eq. (2) is considered to be the ratio of the pressure rise and the distance traveled, Eq. (2) can be

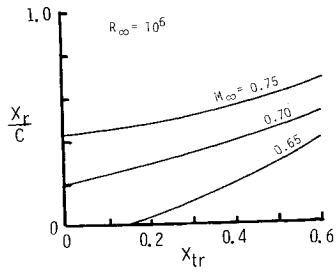

Fig. 2 Variation of ramp break point with transition point location.

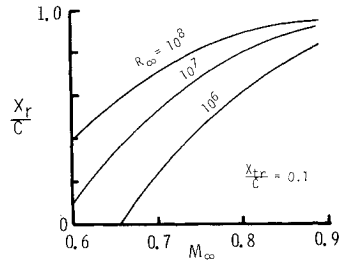

Fig. 3 Variation of ramp break point with freestream Mach number.

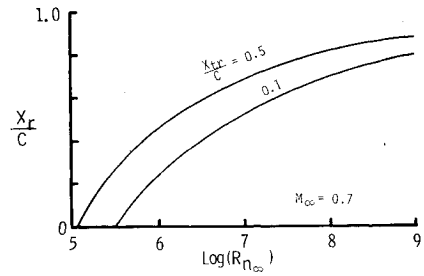

Fig. 4 Variation of ramp break point with Reynolds number.

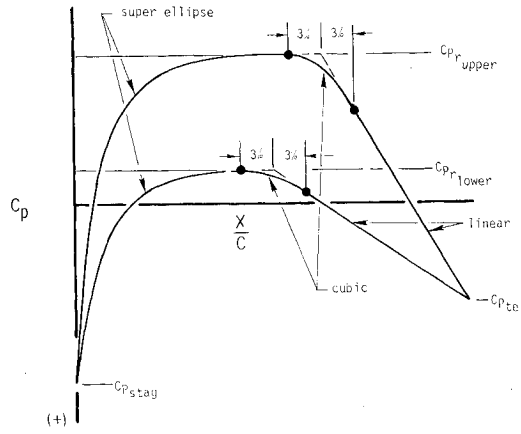

Fig. 5 Pressure distribution model.

rearranged to yield:

$$\bar{C}_{P_{te}} = 1.05[F(1-\frac{X_r}{c})]^{2/n_s} \tag{3}$$

where

$$F = 0.599(10^{-6}R_s)^{0.2}(2^{0.5}(2-n_s))/(x^*/c)_s$$

In Eq. (3) x_r is the ramp break, the chord location where the theoretical recompression begins.

Figure 2 illustrates the variations of x_r/c as a function of the location of the transition point, x_{tr}/c, for three freestream Mach numbers. As the transition point moves aft, the boundary-layer thickness at the trailing edge decreases. As the boundary-layer thickness decreases, the ability to withstand adverse pressure gradients without separating increases. This results in a rearward shift of x_r/c. As the freestream Mach number increases, the ΔC_p required to reach the trailing-edge pressure decreases. This effect also moves the ramp break rearward.

Figure 3 illustrates the influence of freestream Mach number on x_r/c for several Reynolds number values. In this figure transition is fixed at the 10% chord point. As the Mach number increases, the amount of pressure rise from the rooftop value (corresponding to $M_r = 1.03$) to the trailing-edge value ($C_{p_{te}} = 0.2$) is decreased. The thickness of the boundary layer decreases with increasing Mach number. Thus, x_r/c moves aft due to the decreases in boundary-layer thickness and the pressure rise required. The x_r/c point also moves farther aft with increases in Reynolds number. Increases in Reynolds number thins the boundary layer, making possible larger recompression gradients.

Figure 4 shows the variation of x_r/c with Reynolds number for two transition locations. Note that for a fixed transition location there will be a lower limit Reynolds number below which the boundary layer cannot support the recompression gradient.

From Figs. 2-4 the lower bounds of applicability of this type of gradient can be determined. For the case under consideration here, $M_\infty = 0.7$ and $R_N = 2 \times 10^7$, the approach appears to be well suited.

Transition Region

In order to remove the slope discontinuity in the pressure distribution at x_r, a transitional region was inserted between the nose and tail regions. This region was arbitrarily defined as extending from 3% ahead of the x_r/c point to 3% behind it. In this region a cubic curve was used to describe the pressure variation. The slope and ordinates of the cubic were matched to the corresponding values at each end.

Lower Surface

The pressure distribution for the lower surface was prescribed in essentially the same way as for the upper surface pressure. A "super-ellipse" was used for the nose region, a linear recompression for the trailing-edge region, and a 6% chord transitional region was used to connect the two. The exponents for the upper and lower nose pressure distribution equations need not be the same. Obviously, the lower recompression region does not use the Stratford-criterion-based gradient. Also the lower surface C_p must be more positive than the upper surface C_p if the airfoil is to generate lift. The upper and lower surface ramp break points x_r can occur at different chordwise stations.

The composite pressure distribution model is shown in Fig. 5. For the studies presented here, the super-ellipse equations for both upper and lower surfaces used the same value for the exponent n and the same ramp break points. In this case, for a reasonably high value of the exponent n, an approximation to the section lift coefficient is given by:

$$c_l = (C_{p_l} - C_{p_u})x_r + 1/2\,(C_{p_l} - C_{p_u})(1 - x_r)$$
$$= \Delta C_p (x_r + 1)/2 \tag{4}$$

Equation (4) can be used to approximate the lower surface pressure coefficient required to generate a desired value of section lift coefficients.

Analysis Tools

The Bauer-Garabedian-Korn and the Carlson design programs were tested in-house. Of the two, the Carlson program (TRANDES)[4] was found to be easier to use and to modify, in addition to providing answers of adequate accuracy. For this study, the TRANDES-required input of C_p vs x/c was more compatible with our pressure distribution model. (The Bauer, Garabedian, and Korn program required

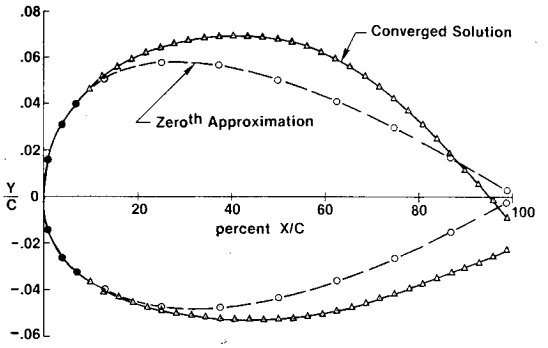

Fig. 6 Initial and final airfoil shapes.

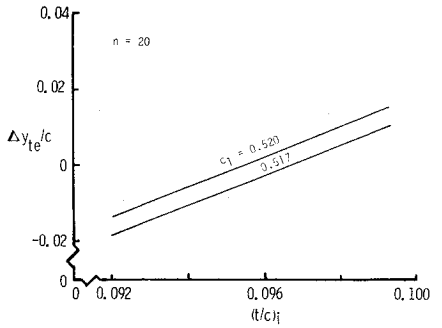

Fig. 7 Trailing-edge closure as a function of initial thickness and design coefficient.

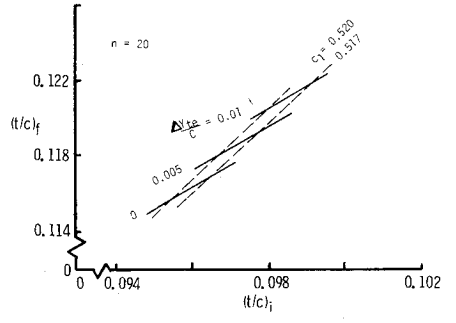

Fig. 8 Final airfoil thickness as a function of initial thickness and design lift coefficient.

C_p as a function of surface distance around the airfoil.) Some difficulties were experienced in running the Bauer-Garabedian-Korn design program at very low Mach numbers. Therefore, on balance, TRANDES was more suitable for our purposes.

Modifications

The TRANDES program uses an initial input airfoil to initiate the design procedure. As the solution progresses, the prescribed pressure distribution is used to determine the geometry of the designed airfoil aft of the first three points on the input airfoil. Thus, the initial airfoil nose shape is retained in the final design airfoil. The initial airfoil is usually taken to be one of the NACA four-digit symmetrical sections.

In order to simplify the usage of TRANDES, a subroutine describing the NACA four-digit airfoil thickness was created and added to the Vought version of the program. Included in this thickness subroutine was a simplified camber consisting of a cubic fore part and a linear rear part. The cubic camber had a zero ordinate at the nose and matched ordinate, slope, and curvature at its juncture with the straight line. The ordinate and location of this match point were under the control of the user. The use of a small amount of camber (on the order of 0.5%) was necessary to reduce pressure "spikes" in

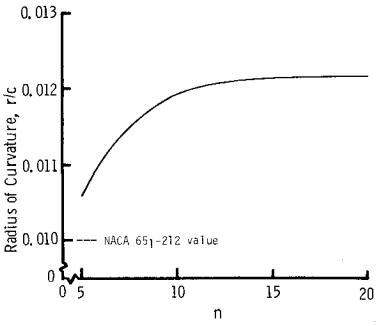

Fig. 9 Variation of leading-edge radius of curvature with exponent n.

Fig. 10 Performance-tailored contour designed for $c_l = 0.52$ at $M = 0.70$.

transitioning from the prescribed geometry to the prescribed pressure distribution. Figure 6 illustrates the connection between the "zeroth" approximation and final converged airfoils. Note that the first three points on both upper and lower surfaces are common to both airfoils.

A second subroutine was also generated which described the desired pressure distribution for TRANDES. Thus the user had only to prescribe C_{p_r}, n, x_r, and $C_{p_{te}}$ for the upper and lower surfaces to completely determine a pressure distribution.

Results

As discussed above, the upper surface Mach number was limited to 1.03 for this study. A value of 0.2 was used for $C_{p_{te}}$ throughout. The design case was taken to be $M_\infty = 0.7$, $R_N = 2 \times 10^7$, and $C_L = 0.52$. Assuming boundary-layer transition at 10% x/c, the Stratford criterion provides an x_r/c value of 0.58.

Using Eq. (4) together with the data specified above, a first approximation for $C_{pr_{\text{lower}}}$ was determined. These descriptions were used to describe the pressure distribution. The t/c of the original NACA section (which sets the first three points on the body) was varied until closure at the trailing edge was obtained. The c_l for this section was checked against the desired c_l and adjustments to $C_{pr_{\text{lower}}}$ were made as necessary. After the first few cases this process proceeded rapidly due to the linearity of the data.

Figure 7 is a working plot showing the variation of trailing-edge closure with initial thickness ratio for two values of section c_l. Due to the linearity of these curves, only two solutions were required to meet closure after the first few solutions.

The connection between initial and final t/c values is shown in Fig. 8 for both zero- and finite-thickness trailing-edge airfoils. It appears from the limited data that the pressure distribution model results in a unique combination of t/c and nose radius for each design.

Figure 9 shows the variation of nose radius with "super-ellipse" exponent n. As n increases from 5 to 20 the nose radius increases to a limit of approximately 1.2% t/c. This limit is due to the interaction of the TRANDES program and the super-ellipse nose pressure distribution. As the value of the exponent n increases, the point on the chord where the local pressure becomes essentially equal to C_p moves rapidly toward the nose. However, the geometric location of the first three nose points must be prescribed when using TRANDES.

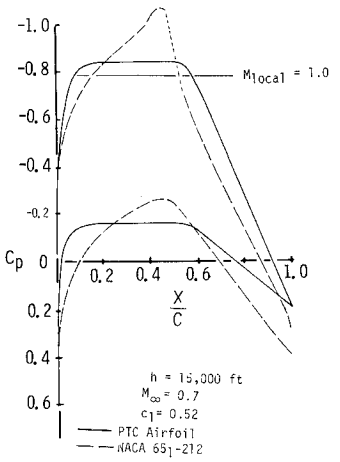

Fig. 11 Comparison of the PTC and NACA 65_1-212 airfoil pressure distributions.

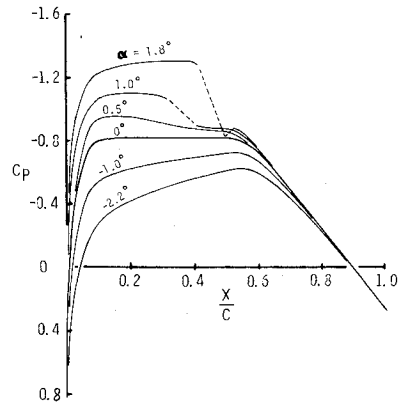

Fig. 12 PTC airfoil upper surface pressure distribution variation at various angles of attack.

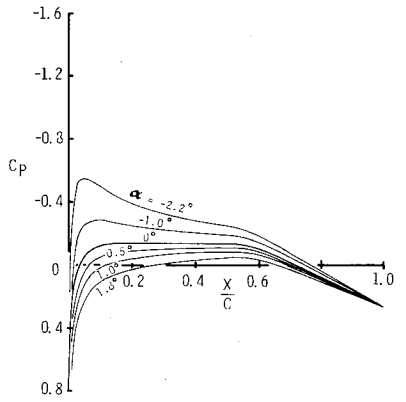

Fig. 13 PTC airfoil lower surface pressure distribution at various angle of attack.

Thus, for n greater than about 28 and the last fixed point at about 6% chord, TRANDES will see no change in the nose pressure distribution.

A resulting performance-tailored contour (PTC) airfoil is presented in Fig. 10 where it is compared with an NACA 65_1-212 airfoil. This PTC airfoil has a nose radius of curvature 20% larger than that of the 6-series airfoil and a larger trailing-edge angle. The PTC airfoil camber is 1.6% at 55% chord.

Figure 11 shows the calculated pressure distribution for the same two airfoils at identical coefficients. The 6-series airfoil develops a very low minimum upper surface pressure coefficient. This flow is then recompressed through a shock wave.

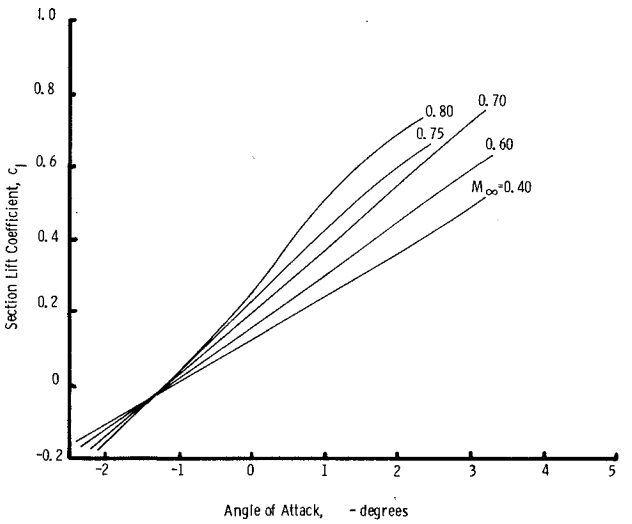

Fig. 14 Section lift coefficient as a function of angle of attack and Mach number.

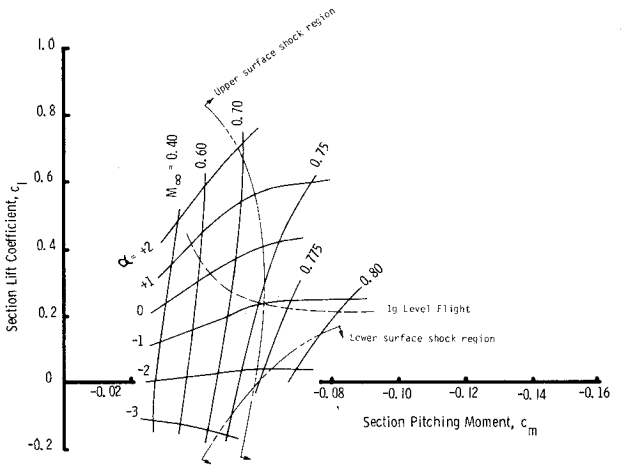

Fig. 15 Variation of pitching moment with lift coefficient for various Mach numbers.

The PTC airfoil pressure distribution matches the design shape and generates no shock waves.

Figure 12 shows the variation in the upper surface pressure distribution of the PTC airfoil over an angle-of-attack range corresponding to a c_l range of 0.15-0.87. (Note that $\alpha = 0$ corresponds to the design case at $M_\infty = 0.7$.) No attempt was made to define the maximum lift capability due to lack of time and proper tools. Up through the design case, $\alpha = 0$, the pressure distribution changes smoothly. At $\alpha = 0.5$ deg, some early recompression occurs in the 20-40% chord region. At 1.0 and 1.8 deg, shocks are clearly in evidence. Note that the pressure gradient near the trailing edge is almost invarient with angle of attack. This appears to support the thesis that separation will occur much later on this type of airfoil than on standard sections.

Figure 13 presents the corresponding lower surface pressures. There are no indications of shock-wave formation. The trailing-edge pressure gradient does appear to be a weak function of angle of attack.

The PTC airfoil lift curves for several Mach numbers are shown in Fig. 14. Above $M_\infty = 0.7$, the lift curves become significantly nonlinear, due to appearance of shocks in the flowfield. For the design case, $c_l = 0.52$ and $M_\infty = 0.7$, there is an absence of any unusual slope changes, thus indicating a well-behaved airfoil.

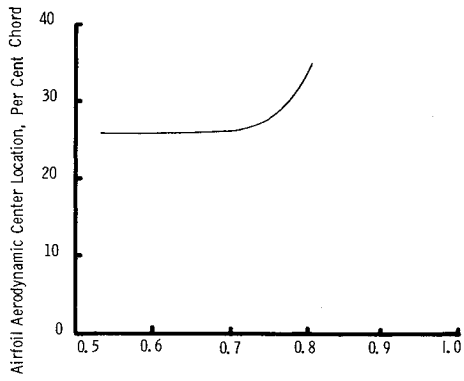

Fig. 16 Variation of airfoil aerodynamic center with Mach number.

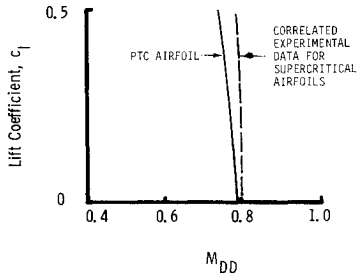

Fig. 17 Variation of M_{DD} with c_l.

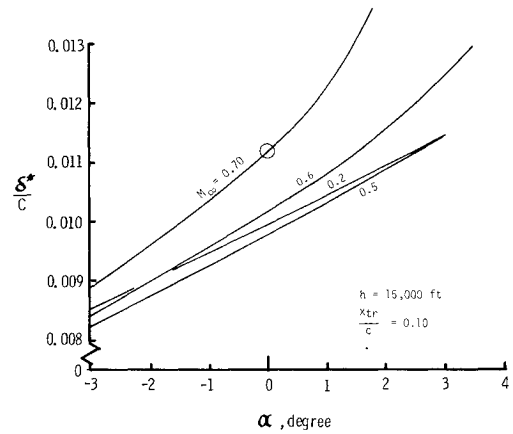

Fig. 18 Trailing-edge boundary-layer growth with angle of attack.

Figure 15 shows the variation of pitching moment with lift coefficient for several Mach numbers. As for the lift curves, significant nonlinearities occur only above $M_\infty = 0.70$. Again, the design point $c_l = 0.52$ and $M_\infty = 0.7$ occurs within the linear region. Approximate boundaries for regions where upper and lower shock waves appear are shown. Along these boundaries, the shock waves are very weak. Their strength increases with both angle of attack and Mach number. For strong shock waves, the TRANDES program has difficulty in treating the shock-boundary layer interaction. Therefore, results for the larger angles of attack at the higher Mach numbers are not shown in Fig. 15.

The level flight C_L line is indicated in Fig. 15 for the study aircraft at maximum weight. Note that the aircraft operating line remains everywhere below the region of significant nonlinearity. There is an aft shift of the airfoil aerodynamic center. This is illustrated in Fig. 16. At low Mach numbers, the *ac* is located at about 26% *c*. Above $M_\infty = 0.7$ the *ac* begins to move rearward in a smooth fashion. At $M_\infty = 0.8$, the *ac* is located at about 34% *c*.

Figure 17 compares the drag divergence Mach number for the PTC airfoil with some Vought-developed correlation for supercritical-type airfoils. The M_{DD} value for the PTC airfoil is 0.785 at zero lift, which compares favorably with the 0.80 value for supercritical types. As the lift coefficient increases, the decrease of M_∞ for the PTC airfoil is somewhat greater than that for the supercritical types. Note that at $c_l = 0.52$, the PTC M_{DD} is still greater than the design Mach number of 0.7.

Figure 18 shows the boundary-layer displacement thickness at 99% chord as a function of angle of attack for several Mach numbers. All calculations were carried out for an altitude of 15,000 ft and the Reynolds numbers are therefore proportional to Mach number. For $M_\infty = 0.2$ and 0.5 there is no rapid thickening indicative of incipient separation. For $M_\infty = 0.6$, the thickness begins to increase somewhat more rapidly above an angle of attack of 1 deg. At $M_\infty = 0.7$ the thickness appears to grow rapidly above the design angle of attack and indicates that separation will occur at slightly larger angles of attack.

Technical Concerns

This paper has outlined a design procedure for a special class of airfoils. Several areas need additional work. Some of these areas of concern are:

1) Nose shape. The NACA four-digit thickness distribution has a square root-type nose shape. The nose radius of curvature is a fixed function of the airfoil thickness. We have investigated a new thickness distribution,

$$2y = a_0\sqrt{x} + a_1 x + a_2 x^2 + a_3 x^3 + a_4 x^4 \tag{5}$$

subject to the following conditions: a specified radius of curvature at the nose, maximum thickness at a specified chord point, and zero curvature at the trailing edge. Using this as the "zeroth approximation" airfoil, significant increases in leading-edge radius are possible. The first examples using this approach have been very encouraging.

2) Calculation grid influence. The default values in TRANDES for the grid generation were used in this study. The influence of changing these coefficients needs to be determined, particularly with regard to very large nose radii.

3) Wave drag. A trustworthy method of determining the wave drag contribution is needed. Dr. Leland Carlson has informed us that this work is in progress.

4) Maximum lift coefficient. The limiting lift coefficients need to be determined. Some analytic capability exists in this area, but to date, it appears to be more of an art than a science.

5) Experimental verification. This is the "proof of the pudding." In spite of problems in generating and interpreting experimental data, it still remains the principal source of proof in this day of computers. Both two- and three-dimensional tests are needed.

Conclusions

This study shows that specialized airfoils can be developed at modest costs to meet special needs. The understanding of fluid flow phenomena has advanced to the point where criteria such as those of Stratford provide the missing link between design requirements and airfoil geometry.

The example airfoil shown here appears to meet the criteria laid out for it. Additional analytical and experimental work are needed to verify these preliminary results.

References

[1]Bauer, F., Garabedian, P., and Korn, D., "Supercritical Wing Section," *Lecture Notes in Economics and Mathematical Systems,* No. 66, Springer Verlag, Berlin, 1972.

[2]Carlson, L.A., "Transonic Airfoil Flowfield Analysis Using Cartesian Coordinates," NASA CR-2577, 1975.

[3]Bauer, F., Garabedian, P., and Korn, D., "Supercritical Wing," Secs. III, *Lecture Notes in Economics and Mathematical Systems,* No. 150, Springer Verlag, Berlin, 1977.

[4]Carlson, L.A., "Transonic Airfoil Design Using Cartesian Coordinates," NASA CR-2578, 1976.

[5]Liebeck, R.H., "On the Design of Subsonic Airfoils for High Lift," Paper 76-406 presented at AIAA 9th Fluid and Plasma Dynamics Conference, San Diego, Calif., July 14-16, 1976.

[6]Anon, "Drag-rise Mach Number of Airfoils Having a Specific Form of Upper-Surface Pressure Distribution: Charts and Comments on Design," EDS Item 771019, Engineering Sciences Data Unit, London, 1971.

[7]Stratford, B.S., "The Prediction of Separation of the Turbulent Boundary Layer," *Journal of Fluid Mechanics,* Vol. 5, Pt. 1, Jan. 1959, pp. 1-16.

[8]Wilkinson, D.H., "Application of Stratford's Turbulent Boundary Layer Criterion to Linear and Maximum Pressure Rises," Hawker Siddley Aviation, Ltd., D.H. Aero Dept./5242/-DHW/GEN/FM, Oct. 1964.